HOKKAIDO UNIVERSITY

Title	Fuel Regression Characteristics in Hybrid Rockets Using Nitrous Oxide/High-Density Polyethylene
Author(s)	Ito, Seiji; Kamps, Landon; Nagata, Harunori
Citation	Journal of propulsion and power, 37(2), 342-348 https://doi.org/10.2514/1.B37875
Issue Date	2021-03
Doc URL	https://hdl.handle.net/2115/81670
Type	journal article
File Information	JPP_for_submittion.pdf

Hokkaido University Collection of Scholarly and Academic Papers : HUSCAP

Fuel Regression Characteristics in Hybrid Rockets Using N_2O/HDPE

Seiji Ito [1], Landon Kamps [2] and Harunori Nagata [3]
Hokkaido University, Sapporo, 060-8628, Japan

Nomenclature

a, A, B, n, m	=	empirical constants
d	=	(inner) diameter, mm
G	=	mass flux, kg/(s-m^2)
L	=	fuel length, m
$\dot{m}$	=	mass flow rate, kg/s
M	=	fuel mass, kg
P	=	pressure, Pa
$\dot{r}$	=	fuel regression rate, mm/s
R, r	=	fuel outer radius, fuel port radius, m
t	=	time, s
T	=	temperature, K
ϕ	=	equivalence ratio
ρ	=	density, kg/m^3

Subscripts

b	=	(burn) time
c	=	chamber position

Presented as Paper 2019-4120 at the AIAA Propulsion and Energy 2019 Forum, Indianapolis, IN, 19-22 August 2019.
[1] Master's course student, Department of Mechanical and Space Engineering, Member AIAA.
[2] Specially Appointed Assistant Professor, Faculty of Engineering, Department of Mechanical and Space Engineering, Member AIAA.
[3] Professor, Faculty of Engineering, Department of Mechanical and Space Engineering, Member AIAA.

i = initial

f = final

ox = oxidizer

p = (fuel) port

t = (nozzle) throat

I. Introduction

In the design of a hybrid rocket motor, the propellant mass flow rates must be adjusted to achieve the required thrust and equivalence ratio. In the most common hybrid rocket configurations, it is possible to throttle the oxidizer because the oxidizer is supplied to the motor as a liquid (or gas), but the fuel cannot be throttled directly in the same way because it is stored in the solid phase. The fuel mass flow rate depends on the fuel regression rate, which is controlled by a diffusion-limited combustion mode such that gasified fuel and oxidizer mix and burn in a turbulent boundary layer formed along the fuel surface. Marxman et al. first demonstrated this in Refs. [1, 2]. The most widely used empirical expression of Marxman et al.'s model is Eq. (1):

$$\dot{r}=aG_{ox}^{n} \tag{1}$$

Where the theoretical value of exponent n is 0.8 for turbulent flow and 0.5 for laminar flow.

Numerous papers report experimental results for a and n under various oxidizer/fuel combinations: e.g. with oxygen (O_2), nitrous oxide (N_2O), or hydrogen peroxide (H_2O_2) as oxidizers; and polyethylene (PE)-, polybutadiene (PB)- or polypropylene (PP)-based rubbers and plastics as fuels. There are few papers reporting the characteristics of N_2O and High-Density PE (N_2O/HDPE) combustion and the corresponding fuel regression rate formula, even though this propellant combination has great potential for commercial use given its low cost, widespread availability, storability at room temperature, non-toxicity, and self-pressurizing potential [3]. Only two empirical correlations for this propellant combination were found in a literature review, each with differing results: Doran et al. report a = 0.116 and n = 0.33 [4], and Kamps et al. report a = 0.0436 and n = 0.62 [5] where fuel regression rate has units of mm/s and oxidizer mass flux has units of kg/m^2-s.

The effect of radiant heat, which is excluded in the formulation of Eq. (1), is a possible explanation for the varying results of Refs. [4,5]. Chiaverini et al. derived a fuel regression formula that includes radiant heat effects [6]. The major obstacle to implementing this regression formula is that it requires knowledge of the chemical decomposition of the fuel, in addition to four curve fitting constants and the emissivity of the resulting combustion gas.

The main objective of this study is to determine the fuel regression rate formula of a hybrid rocket motor using N_2O and HDPE through experimentation. A secondary objective is to offer an explanation for the differing results of previous research by investigating the possible dependencies of fuel regression rate on chamber pressure and equivalence ratio, which are expected to capture the effect of radiant heat.

II. Method

It is not clear from Refs. [4-6] whether the fuel regression rate formula for N_2O/HDPE hybrid rocket motors has some pressure or equivalence ratio dependency, as observed in hybrid rockets using other propellant combinations due to the effect of radiant heat. This is mostly due to a lack of fuel regression data that varies in pressure and equivalence ratio, but also because these correlations were based on time-averaged changes in fuel port diameter. The concept of this study is to accurately determine the empirical coefficients of Eq. (1), as well as two additional models that include radiant heat effects, by conducting firing tests at various oxidizer mass fluxes while controlling for chamber pressure. Furthermore, an integral-method is used for correlating experimental data in place of the more commonly used time-averaged method to improve the accuracy of results.

A. Time-integral Method

In Refs. [4], fuel regression rate was determined by measuring the mass of fuel before and after firing, calculating the overall change in spatially-averaged port diameter based on this change in mass, and dividing by the combustion time. This procedure is referred to as the time-averaged method. The equation for determining fuel port diameter from fuel mass before and after firing is shown by Eq. (2):

$$r_i = \sqrt{R^2 - \frac{M_i}{\pi \rho L}}$$
$$r_f = \sqrt{\frac{M_i - M_f}{\pi \rho L} + r_i^2} \tag{2}$$

As is evident from Eq. (1), unless very small changes in port diameter take place, these time-averages fail to capture the non-linear dependency of fuel regression on oxidizer mass flux. Furthermore, if nozzle throat erosion occurs, leading to a decrease in chamber pressure during firing, the inaccuracy of time-averaged correlations including chamber pressure are further exacerbated. The same is true when including an equivalence ratio term in the empirical formula because some amount of mixture ratio shifting occurs during firing if exponent n is not equal to 0.5. A correlation based on the time-integral of the fuel regression formula under review eliminates this problem and requires no additional measurements. For example, Eq. (3) shows the time-integral form of Eq. (1) for correlation.

$$\begin{gathered} \frac{dr}{dt}=aG_{ox}^{n} \\ \frac{\pi^{n}}{2n+1}\left(r_{f}^{2n+1}-r_{i}^{2n+1}\right)=a\int_{0}^{t_b}\dot{m}_{ox}^{n}dt \cong a\sum_{t=0}^{t_b}\dot{m}_{ox}^{n}\Delta t \end{gathered} \tag{3}$$

A detailed analysis of the time-integral method and its improvement over the time-average method is summarized by Rabinovitch et al. in Ref. [7].

B. Models for Empirical Correlation

Three empirical models are considered in this research as a way to test the functional dependencies of fuel regression rate on pressure and equivalence ratio, as shown in Table 1. Model 1, listed as Eq. (1), is the simplified empirical form of Marxman's diffusion-limited model and the basis of the correlations in Refs. [4,5]. Model 2, listed as Eq. (4), is the modification to Model 1 that improves accuracy by including the effect of radiant heat through a pressure term with a constant exponent [8,9]:

$$\dot{r}=aG_{ox}^{n}P_{c}^{m} \tag{4}$$

In Model 3, only a simple modification is applied to the pressure exponent m of Model 2 (Eq. (4)) to capture the effect of soot-concentration on radiant heat intensity, as shown by Eq. (5):

$$m=A\phi^{B} \tag{5}$$

In very oxidizer-rich conditions (ϕ<<1), the pressure exponent of Model 3 will become negligibly small, which corresponds to the expected non-existence of soot. The pressure exponent increases with the equivalence ratio, which correlates with the expected increase in the concentration of soot. In this way, Model 3 serves as a practical application of findings from previous research that radiant heat from soot accelerates fuel gasification, and this effect is exponentially dependent on both chamber pressure and O/F ([10 p. 58]). The empirical coefficients in Eq. (5) and exponent *n* are determined at the same time by the least-squares method.

C. Experimental Measurement and Setup

Figure 1 is a simplified schematic of the experimental apparatus. The experimental apparatus consists mainly of a tank of gaseous Ar for feed pressure, a reservoir of liquid N_2O for the oxidizer, a tank of gaseous O_2 as an alternative "bypass" oxidizer for ignition, a tank of gaseous N_2 as a purging agent, an orifice for measuring the oxidizer mass flow rate, and the motor assembly. The firing sequence was controlled using LabVIEW7. The pressure upstream and downstream of the orifice, downstream of the Ar tank regulator, and in the combustion chamber were measured using KYOWA pressure sensors. The thrust during firing test was measured using KYOWA LMA-A-200N load cell for tests less than 200 N and LMA-A-500N load cell for tests more than 200 N. Figure 2 shows a detailed schematic of firing test motor with a typical fuel grain. Liquid N_2O, which is pressurized by Ar, is supplied to the motor in the axial direction through injectors with 2-4 x 0.8 mm holes that impinge at an angle of 90 deg. The nozzle throat diameter was varied from 4–7.6 mm, and the nozzle expansion ratio was varied from 3–9 between tests. The fuel grain consists of 6-10 cylindrical fuel blocks, and the aft mixing chamber consists of 1-4 cylindrical graphite blocks. All blocks were 20–22 mm long, with outer diameters of 47 mm. Initial fuel block port diameters were 10, 20, and 30 mm, and aft mixing chamber block port diameters were 30 mm.

The oxidizer mass flow rate is measured by the pressured drop across the orifice upstream of the injector. The density of nitrous oxide is a function of temperature which is calculated based on the NIST database [11]. In the first second that N_2O is supplied to the test motor, the flow in the supply line becomes a saturated liquid (two-phase mixture of liquid and vapor). During this time, the oxidizer mass flow rate cannot be measured accurately using the orifice. The phase of oxidizer at injection can be inferred from the pressure measurement downstream of the orifice. The influence of an inaccurate measurement of the oxidizer mass flow rate during this initial transient on empirical correlations for the regression rate is evaluated in the following section (Ⅲ.C. Sensitivity Analysis).

The high-density polyethylene rods used to manufacture fuel blocks for this study were purchased from Takada Chemical Corporation and measured to have a density of 955 ± 5 kg/m^3. Although Heister and Wernimont reported that widely varying grades of polyethylene may result in different fuel regression characteristics [12], such effects are not considered in comparison with previous studies. A similar comparison focusing only on differences in HDPE as manufactured by different suppliers would be costly, and it is not obvious that the effect of HDPE manufacturing processes and related material properties would have an effect on par with that of the main parameters of Marxman's model, mainly oxidizer port mass flux. Furthermore, even if HDPE manufacturing processes lead to significant variations in fuel regression characteristics, these effects on the fuel regression rate will be captured by the empirical coefficients that are subject to investigation in the empirical models of this study.

III. Results and Discussion

In total, 29 static firing tests were conducted for this study: ranging from 0.7 to 2.3 in equivalence ratio, from 1.1 MPa to 5.0 MPa in chamber pressure, and from 40 kg-s^{-1}-m^{-2} to 240 kg-s^{-1}-m^{-2} in oxidizer port mass flux. The results for all tests are listed in Tables 2 and 3. Double and triple asterisks are used to distinguish the tests in which the accuracy of the orifice flow rate measurement is unclear because the flow is likely a saturated liquid of undeterminable quality for a relatively large portion of firing, and the evaluation of this uncertainty is outside the purview of the analysis of Section III.C. In 6 of the 29 tests, the pressure downstream of the orifice was equal to or below the vapor pressure of N_2O as determined by temperature and pressure measurements upstream of the orifice during the entire firing. This implies that the Ar (feed) pressure and orifice size were inappropriately matched to ensure N_2O could be supplied as a compressed liquid for the given flow rate. A similar pressure disparity occurs partway into 7 additional firing tests due to a chamber pressure decreases that result from nozzle throat erosion. Figure 3 shows pressure histories from two tests representing each of these two cases: Ar pressurization was insufficient in Test 11; and nozzle throat erosion causes a significant decrease in chamber pressure in Test 4.

After excluding the 13 tests in which the accuracy of the oxidizer mass flow rate is unknown, there are 16 tests remaining for empirical correlation. Figure 4 shows the results of Test 2 as a representative firing test for empirical analysis. The thrust and chamber pressure sharply rise within the first 0.5 seconds, then gradually approach a steady state. The Ar tank pressure and orifice upstream pressure are almost the same. In most cases, the chamber pressure gradually decreases due to nozzle throat erosion. The combustion duration was determined by the standards outlined

in Ref. [13]. In Fig. 3, some degree of two-phase flow occurs during the first 0.5 seconds of firing. When N_2O is supplied as a liquid, the pressure is maintained above the vapor pressure up to the injector through external pressurization by Ar in the N_2O reservoir.

Three empirical models are considered in this study, where Models 2 and 3 include pressure and/or equivalence ratio dependency terms that are intended to capture the effects of radiant heat. All empirical coefficients in Models 1 thru 3 are determined by the least-squares method and the time-integral method. The empirical coefficients and the coefficients of determination of all empirical models are shown in Table 4.

A. Direct Comparison with Previous Research Results

Figure 5 shows the relationship between the fuel regression rate and oxidizer port mass flux in this study and previous studies according to Model 1. The dotted and solid black trend lines are the results of Model 1 correlations from this study obtained by the time-averaged and time-integral methods, respectively. The empirical coefficients a and n of the time-averaged method from 16 tests are $a = 0.0163$ and $n = 0.74$ with a coefficient of determination of merely 0.43. These values become $a = 0.0763$ and $n = 0.42$ with a coefficient of determination of 0.85 using the integral method. This shows that the time-integral method based on Eq. (1) produces much more accurate results than the time-averaged method. The results of the time-integral correlation of Model 1 are plotted in Fig. 6. Note that the correlation is conducted using only the 16 tests for which oxidizer mass flow rate accuracy could be evaluated. These 16 tests are shown by solid black markers. For reference purposes, the data from the remaining "13 excluded tests" were also plotted, using hollow black markers to distinguish them from the correlation data.

The red dotted line of Fig. 5 is the result of Doran et al. [4], and the blue dotted line of Fig. 5 is the result of Kamps et al. [5]. The result of Doran et al. is in good agreement with the result obtained in this study, however, the empirical coefficients do not match. In addition, it is thought that these empirical formulas do not explain the physical phenomenon, because oxidizer port mass flux exponents from both formulas are less than the theoretical minimum value (0.5). On the other hand, the result of Kamps et al. obviously disagree with the result of this study. One reason for this discrepancy may be the limited range of oxidizer port mass flux, pressure, and equivalence ratio values observed in Kamps et al.'s study. In the empirical analysis done by Kamps et al., time-averaged values of oxidizer port mass flux, chamber pressures and equivalence ratios were consistently around 60 kg/m^2-s, 4 MPa and 2.0, whereas these values vary greatly between tests in this study.

Another interesting finding from the comparison with Doran et al.'s results is that values agree well even though the injector conditions vary greatly. Carmicino and Sorge demonstrated that the flow conditions induced by the injector can influence the fuel regression rate significantly [14]. In this study, N_2O streams converge into a single impinging stream, whereas in Doran et al.'s study, N_2O streams are injected in straight or diverging showerhead configurations. Furthermore, the shape of the fuel port entrance was customized for the ignitor. Although the injectors and the fuel shape just below the injectors are different between Doran et al.'s apparatus and the apparatus of this study, the fuel regression rates are almost the same when conditions of oxidizer port mass flux, pressure, and equivalence ratio are the same (i.e. Tests 1-3). This suggests that the influence of the injector cannot adequately explain the discrepancies in the results of the remaining tests in the following sections.

B. The Effect of Radiant Heat

Figure 7 shows the time-integral correlation of Model 2, which contains the effect of chamber pressure as the radiant heat term. The empirical coefficients a, n and m are $a = 0.0308$, $n = 0.53$ and $m = 0.43$ respectively. The coefficient of determination of Model 2 improved compared to that of Model 1 (for 16 tests data), from R2 = 0.85 to R2 = 0.95. Figure 8 shows the results of the time-integral correlation of Model 3. The empirical coefficients a, n, A and B are $a = 0.0298$, $n = 0.52$, $A = 0.52$ and $B = -0.14$ respectively. The results show that the accuracy is not improved over the slightly simpler formula of Model 2, even though there is an additional fitting constant in the exponent of the pressure term. The fact that the accuracy remained the same between Models 2 and 3 may simply be the consequence of a lack of data sets for which chamber pressure and equivalence ratio vary independently. It is clear from Table 3 that although there is great variance in both equivalence ratio and chamber pressure between tests, these terms vary in unison. This is a reflection on the difficulty of conducting tests where interdependent terms are attempted to be controlled and made to vary independently. Thus, the efficacy of Model 3 remains inconclusive.

C. Sensitivity Analysis

Table 5 lists the results of sensitivity analysis of the empirical coefficients of Models 1-3 with respect to the experimental data of chamber pressure, oxidizer mass flow rate, and fuel mass consumption. Here, each of the three sets of input data was increased by 5%, and the empirical coefficients of each model were recalculated using the same least-squares algorithm. The resulting changes in the value of the empirical coefficients were used to approximate the partial derivative terms of Table 5. The measurement uncertainty terms U_{x_i} were chosen to be the accuracy of the

sensors used to measure experimental values of terms x_i . The numerical results of Table 4 are listed as percentages of the nominal mean value. Since input data were varied by 5%, any terms less than 5% suggest a low sensitivity, and terms greater than 5% suggest a high sensitivity. The results show that all empirical coefficients are generally unaffected by perturbations in the experimental data.

Moreover, another sensitivity analysis was done to investigate how inaccurate measurements of oxidizer mass flow rate during the initial transients affect the results of the empirical correlation. The sensitivity analysis is done by evaluating the fluctuation when the oxidizer mass flow rate during the transient is assumed to be a constant minimum value obtained from experimental flow tests. The results of this sensitivity analysis are listed in Table 6. The results show that inaccurate measurements of oxidizer mass flow rate during the initial transients do not significantly affect the empirical formula. Fig. 9 shows the oxidizer mass flow rate history under the assumption in Test 16. The nominal value of N_2O flow rate used in empirical correlations is a reliable "maximum" value during the transient because it is based on the assumption of incompressible (compressed) liquid flow across the orifice. The minimum flow rate $\dot{m}_{ox}^{*}$ are measured by conducting N_2O flow tests that only used the mainline of Fig. 1 without test motor (the downstream at the orifice was opened to the atmospheric pressure). This basis for sensitivity analysis is appropriate because the flow line is opened to the atmosphere at the beginning of ignition. Since in this configuration N_2O is completely vaporized in vicinity of the orifice, this assumption for a constant value of (vaporized) N_2O mass flow rate during the initial transient serves as a reliable "minimum" value.

IV. Conclusion

There are few publications about the fuel regression rate of the hybrid rocket propellant combination nitrous oxide and high-density polyethylene (N_2O/HDPE). The results of all two existing studies, one of which considers only time-averaged fuel regression rates, differ from one another. In this research, the fuel regression rates of hybrid rocket motors using the propellant combination N_2O/HDPE are determined through 16 static firing test results and compared with values observed in previous research due to the deference of the experimental conditions between studies, and the effect of the time-averaged method used in previous research. The time-integral method of the fuel regression rate is shown to greatly improve the accuracy of empirical correlations over the time-averaged approach, increasing the coefficient of determination from 0.42 to 0.85. It was found that modifying the basic empirical formula of Marxman et al.'s diffusion-limited model approximation by including a chamber pressure term further increased the coefficient

of determination to 0.95. When the chamber pressure exponent is assumed to exhibit an equivalence ratio dependency, the effect of the equivalence ratio was not observed well.

Acknowledgment

This research is supported by the Japanese Ministry of Education, Culture, Sports, Science and Technology as: Grant-in-Aid for Scientific Research (B) 19H02336 and by a matching fund program of Centers for Inter-University Collaboration from ISAS (Institute of Space and Aerospace Exploration Agency)

References

[1] Marxman, G. and Gilbert, M., "Turbulent Boundary Layer Combustion in the Hybrid Rocket," *Symposium (International) on Combustion*, Vol. 9, No. 1, 1963, pp. 371-383.
doi: https://doi.org/10.1016/S0082-0784(63)80046-6

[2] Marxman, G., Wooldridge, C. and Muzzy, R., "Fundamentals of Hybrid Boundary-Layer Combustion," *Heterogeneous Combustion*, edited by Glassman, I., Green, L. and Wolfhard, H., Vol. 15, Progress in Astronautics and Rocketry, AIAA, 1964, pp. 485-522.
doi: https://doi.org/10.2514/5.9781600864896.0485.0522

[3] Heister, S. and Wernimont, E., "Hydrogen Peroxide, Hydroxyl Ammonium Nitrate, and Other Storable Oxidizers," *Fundamentals of Hybrid Rocket Combustion and Propulsion*, edited by M. Chiaverini and K. Kuo, Vol. 218, Progress in Astronautics and Aeronautics, AIAA, Reston, VA, 2006, pp. 457-487.
doi: https://doi.org/10.2514/5.9781600866876.0457.0488

[4] Doran, E., Dyer, J., Lohner, K., Dunn, Z., and Cantwell, B., "Nitrous Oxide Hybrid Rocket Motor Fuel Regression Rate Characterization," *43rd AIAA/ASME/SAE/ASEE Joint Propulsion Conference and Exhibit*, AIAA Paper 2007-5352, July 2007.
doi: https://doi.org/10.2514/6.2007-5352

[5] Kamps, L., Sakurai, K., Saito, Y., and Nagata, H., "Comprehensive Data Reduction for N_2O/HDPE Hybrid Rocket Motor Performance Evaluation," *Aerospace*, Vol. 6, No. 4, 2019, 45.
doi: https://doi.org/10.3390/aerospace6040045

[6] Chiaverini, M., Kuo, K., Peretz, A., and Harting, G., "Regression-Rate and Heat-Transfer Correlations for Hybrid Rocket Combustion," *Journal of Propulsion and Power*, Vol. 17, No. 1, 2001, pp. 99-110.
doi: https://doi.org/10.2514/2.5714

[7] Rabinovitch, J., Jens, E., Karp, A., Nakazono, B., Conte, A., and Vaughan, D., "Characterization of PolyMethylMethAcrylate as a Fuel for Hybrid Rocket Motors," 54th *AIAA/ASME/SAE/ASEE Joint Propulsion Conference and Exhibit*, AIAA Paper 2018-4530, July 2018.

doi: https://doi.org/10.2514/6.2018-4530

[8] Carmicino, C. and Sorge, A., "Role of Injection in Hybrid Rockets Regression Rate Behaviour," *Journal of Propulsion and Power*, Vol. 21, No. 4, 2005, pp. 606-612.
doi: https://doi.org/10.2514/1.9945

[9] Frederick, R., Whitehead, J., Knox, L., and Moser, M., "Regression Rates Study of Mixed Hybrid Propellants," *Journal of Propulsion and Power*, Vol. 23, No. 1, 2007, pp. 175-180.
doi: https://doi.org/10.2514/1.14327

[10] Chiaverini, M., "Review of Solid-Fuel Regression Rate Behavior in Classical and Nonclassical Hybrid Rocket Motors," *Fundamentals of Hybrid Rocket Combustion and Propulsion*, edited by M. Chiaverini and K. Kuo, Vol. 218, Progress in Astronautics and Aeronautics, AIAA, Reston, VA, 2006, pp. 37-126.
doi: https://doi.org/10.2514/5.9781600866876.0037.0126

[11] NIST. Thermophysical Properties of Fluid Systems. Available online: https://webbook.nist.gov/chemistry/fluid/ (accessed on 1 November)

[12] Heister, S., Wernimont, E., "Hydrogen Peroxide, Hydroxyl Ammonium Nitrate, and Other Storable Oxidizers," *Fundamentals of Hybrid Rocket Combustion and Propulsion*, edited by M. Chiaverini and K. Kuo, Vol. 218, Progress in Astronautics and Aeronautics, AIAA, Reston, VA, 2006, pp. 457-487.
doi: https://doi.org/10.2514/5.9781600866876.0457.0488

[13] Sutton, G., and Biblarz, O., "Definitions and Fundamentals," *Rocket Propulsion Elements*, 7th ed., Wiley, Hoboken, NJ, 2000, pp. 27-44.

[14] Carmicino, C. and Sorge, A., "Influence of a Conical Axial Injector on Hybrid Rocket Performance," *Journal of Propulsion and Power*, Vol. 22, No. 5, 2006, pp. 984-995.
doi: https://doi.org/10.2514/1.19528

Table 1 Empirical models

Model name	Model formula
Model 1	$\dot{r}=aG_{ox}^{n}$
Model 2	$\dot{r}=aG_{ox}^{n}P_{c}^{m}$
Model 3	$\dot{r}=aG_{ox}^{n}P_{c}^{m}$ $m=A\phi^{B}$

Table 2 Summary of test data

Test	Direct measurement					
	t_b s	d_t mm	ΔM g	$\overline{\dot{m}_{ox}}$ kg/s	$\overline{G_{ox}}$ kg/(m^{2}s)	$\overline{P_c}$ MPa
Test 1	9.9	6.8	48.4 ± < 1 %	0.055 ± 3 %	114 ± 3 %	2.1 ± 0.9 %
Test 2	9.9	7.2	48.1 ± < 1 %	0.065 ± 5 %	132 ± 5 %	2.0 ± 0.9 %
Test 3	8.5	7.6	46.3 ± < 1 %	0.079 ± 7 %	163 ± 7 %	2.1 ± 0.9 %
Test 4**	10	5.5	39.5 ± < 1 %	0.037 ± 3 %	79 ± 3 %	2.0 ± 0.9 %
Test 5**	10	4.6	36.9 ± < 1 %	0.029 ± 3 %	63 ± 3 %	2.5 ± 0.7 %
Test 6***	5.0	4.0	40.6 ± < 1 %	0.033 ± 5 %	53 ± 5 %	4.1 ± 0.4 %
Test 7***	4.3	4.0	34.9 ± < 1 %	0.034 ± 5 %	56 ± 5 %	4.0 ± 0.5 %
Test 8**	3.6	4.0	29.8 ± < 1%	0.035 ± 5 %	58 ± 5 %	4.0 ± 0.5 %
Test 9**	9.9	4.0	73.9 ± < 1 %	0.033 ± 5 %	48 ± 5 %	4.1 ± 0.4 %
Test 10**	15	4.0	109.9 ± < 1%	0.032 ± 6 %	44 ± 6 %	4.2 ± 0.4 %
Test 11***	10	4.0	73.1 ± < 1 %	0.032 ± 4 %	47 ± 4 %	4.2 ± 0.4 %
Test 12***	10	4.0	74.1 ± < 1 %	0.033 ± 5 %	49 ± 5 %	4.0 ± 0.5 %
Test 13***	10	4.0	54.6 ± < 1 %	0.037 ± 4 %	74 ± 4 %	3.3 ± 0.5 %
Test 14***	15	4.0	78.4 ± < 1 %	0.040 ± 4 %	74 ± 4 %	2.8 ± 0.6 %
Test 15	5.0	4.0	28.2 ± < 1 %	0.036 ± 4 %	79 ± 4 %	3.9 ± 0.5 %
Test 16	5.0	4.0	22.9 ± < 1 %	0.038 ± 4 %	225 ± 4 %	3.9 ± 0.5 %
Test 17	10	4.0	51.4 ± < 1 %	0.039 ± 3 %	201 ± 4 %	3.3 ± 0.5 %
Test 18***	15	4.0	61.6 ± < 1 %	0.041 ± 4 %	207 ± 4 %	2.7 ± 0.7 %
Test 19	10	4.0	49.7 ± < 1 %	0.040 ± 3 %	83 ± 3 %	3.7 ± 0.5 %
Test 20	9.9	5.5	47.8 ± < 1 %	0.044 ± 3 %	92 ± 3 %	2.0 ± 0.9 %
Test 21	9.9	4.0	72.9 ± < 1 %	0.030 ± 4 %	68 ± 4 %	5.0 ± 0.4 %
Test 22	5.0	4.9	24.7 ± < 1 %	0.043 ± 13 %	57 ± 13 %	2.6 ± 0.7 %
Test 23	4.9	6.0	23.8 ± < 1 %	0.041 ± 13 %	53 ± 13 %	1.8 ± 1 %
Test 24	5.0	6.2	23.3 ± < 1 %	0.051 ± 9 %	68 ± 9 %	1.9 ± 1 %
Test 25	5.0	5.8	23.1 ± < 1 %	0.044 ± 9 %	58 ± 9 %	2.0 ± 0.9 %
Test 26	4.9	6.1	21.0 ± < 1 %	0.046 ± 11 %	61 ± 11 %	1.8 ± 1 %
Test 27*	4.9	6.2	17.1 ± < 1 %	0.033 ± 70 %	45 ± 70 %	1.1 ± 1.6 %
Test 28**	5.0	6.2	19.5 ± < 1 %	0.039 ± 15 %	51 ± 15 %	1.4 ± 1.3 %
Test 29	9.9	5.6	68.2 ± < 1 %	0.042 ± 3 %	241 ± 3 %	2.6 ± 0.7 %

* The uncertainty in oxidizer mass flow rate was 70% because the pressure drop across the orifice was small. Since the flow rate is close to the expected value and consistent with the experiment scheme, this data was not discarded.
** Tests in which the pressure downstream of the orifice was equal to or below the vapor pressure of nitrous oxide as determined by pressure and temperature upstream of the orifice as a result of insufficient Ar pressurization.
*** Tests in which the pressure downstream of the orifice decreases to the vapor pressure of nitrous oxide as determined by pressure and temperature upstream of the orifice during firing as a result of nozzle throat erosion.

Table 3 Summary of test results

Test	Analysis			Fuel conditions	
	$\dot{m}_{ox}^{*}$ kg/s	$\bar{\phi}$	$\bar{\dot{r}}$ mm/s	L mm	$d_{p,i}$ mm
Test 1	0.040	0.83	0.51 ± 0.3 %	122	20
Test 2	0.055	0.71	0.50 ± 0.3 %	122	20
Test 3	0.070	0.65	0.57 ± 0.3 %	122	20
Test 4**	-	1.00	0.42 ± 0.4 %	122	20

Test 5**	-	1.19	0.40 ± 0.4 %	122	20
Test 6***	-	2.31	0.59 ± 0.4 %	162	26
Test 7***	-	2.25	0.60 ± 0.4 %	162	26
Test 8**	-	2.27	0.63 ± 0.5 %	162	26
Test 9**	-	2.12	0.50 ± 0.2 %	162	26
Test 10**	-	2.16	0.47 ± 0.1 %	162	26
Test 11***	-	2.13	0.50 ± 0.2 %	162	26
Test 12***	-	2.09	0.50 ± 0.2 %	162	26
Test 13***	-	1.38	0.55 ± 0.3 %	122	20
Test 14***	-	1.25	0.50 ± 0.2 %	122	20
Test 15	0.030	1.49	0.63 ± 0.5 %	122	20
Test 16	0.030	1.13	0.78 ± 0.7 %	122	10
Test 17	0.030	1.26	0.73 ± 0.4 %	122	10
Test 18***	-		0.55 ± 0.3 %	122	10
Test 19	0.030	1.17	0.52 ± 0.3 %	122	20
Test 20	0.030	1.02	0.50 ± 0.3 %	122	20
Test 21	0.030	2.31	0.48 ± 0.2 %	202	20
Test 22	0.055	1.08	0.34 ± 0.6 %	156	30
Test 23	0.055	1.12	0.33 ± 0.6 %	156	30
Test 24	0.055	0.86	0.32 ± 0.6 %	156	30
Test 25	0.055	1.00	0.32 ± 0.6 %	156	30
Test 26	0.055	0.87	0.29 ± 0.7 %	156	30
Test 27*	0.070	0.98	0.24 ± 0.8 %	156	30
Test 28**	-	0.95	0.27 ± 0.7 %	156	30
Test 29	0.030	1.55	0.63 ± 0.3 %	202	10

* The uncertainty in oxidizer mass flow rate was 70% because the pressure drop across the orifice was small. Since the flow rate is close to the expected value and consistent with the experiment scheme, this data was not discarded.
** Tests in which the pressure downstream of the orifice was equal to or below the vapor pressure of nitrous oxide as determined by pressure and temperature upstream of the orifice as a result of insufficient Ar pressurization.
*** Tests in which the pressure downstream of the orifice decreases to the vapor pressure of nitrous oxide as determined by pressure and temperature upstream of the orifice during firing as a result of nozzle throat erosion.

Table 4 Results of empirical correlation

Model name	Model formula	Coefficient of determination
Model 1 (16 tests) time-averaged method	$\dot{r}=0.0163G_{ox}^{0.74}$	$R^2=0.43$
Model 1 (16 tests) time-integral method	$\dot{r}=0.0763G_{ox}^{0.42}$	$R^2=0.85$
Model 2 (16 tests) time-integral method	$\dot{r}=0.0308G_{ox}^{0.53}P_c^{0.43}$	$R^2=0.95$
Model 3 (16 tests) time-integral method	$\dot{r}=0.0298G_{ox}^{0.52}P_c^{m}$ $m=0.52\phi^{-0.14}$	$R^2=0.95$

Table 5 Results of sensitivity analysis

Δx_i	U_{x_i}	Empirical Model	$\frac{U_{x_i}}{a}\frac{\partial a}{\partial x_i}$ [%]	$\frac{U_{x_i}}{n}\frac{\partial n}{\partial x_i}$ [%]	$\frac{U_{x_i}}{m}\frac{\partial m}{\partial x_i}$ [%]	$\frac{U_{x_i}}{A}\frac{\partial A}{\partial x_i}$ [%]	$\frac{U_{x_i}}{B}\frac{\partial B}{\partial x_i}$ [%]
$\Delta\overline{P_c}$ [MPa]	0.0566	Model 1	-	-	-	-	-
		Model 2	-0.9	0.0	0.0	-	-
		Model 3	-0.6	0.0	-	-0.7	-2.7
$\Delta\overline{\dot{m}_{ox}}$ [kg/s]	0.0037	Model 1	-3.5	0.0	-	-	-
		Model 2	-4.3	0.0	0.0	-	-
		Model 3	-3.3	0.0	-	-3.2	0.0
ΔM_f [kg]	0.0001	Model 1	0.2	0.0	-	-	-
		Model 2	0.2	0.0	0.0	-	-
		Model 3	0.5	-0.1	-	0.0	0.3

Table 6 The effect of inaccurate oxidizer mass flow rate measurement on empirical results

Empirical model	$\frac{\Delta a}{a}$ [%]	$\frac{\Delta n}{n}$ [%]	$\frac{\Delta m}{m}$ [%]	$\frac{\Delta A}{A}$ [%]	$\frac{\Delta B}{B}$ [%]
Model 1	11.1	-4.8	-	-	-
Model 2	-0.7	0.0	4.7	-	-
Model 3	-0.3	0.0	-	3.9	-7.1

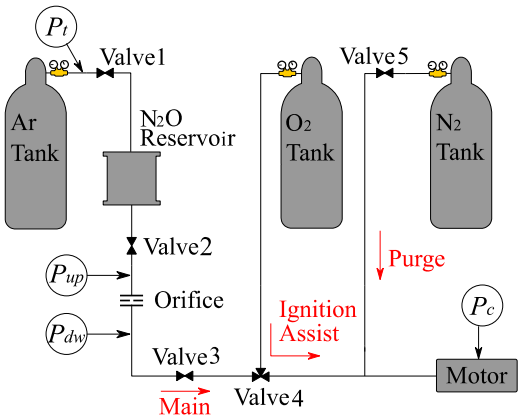

Fig. 1 Schematic of experimental apparatus

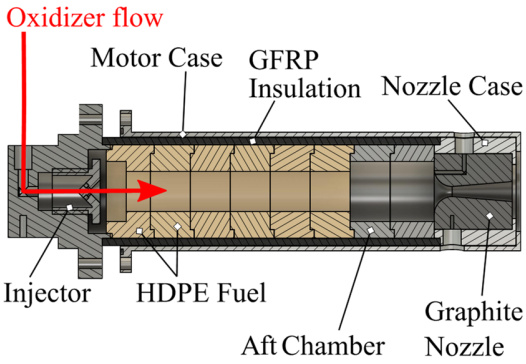

Fig. 2 Details of test motor configuration

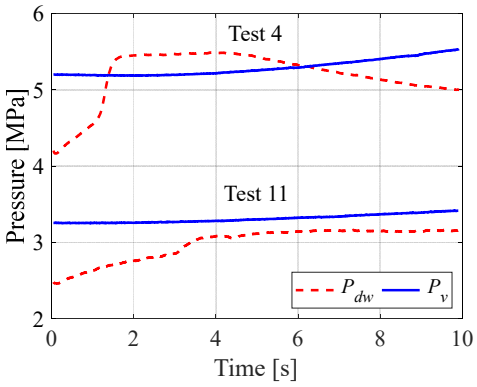

Fig. 3 Two tests in which N_2O flow rate accuracy is unknown

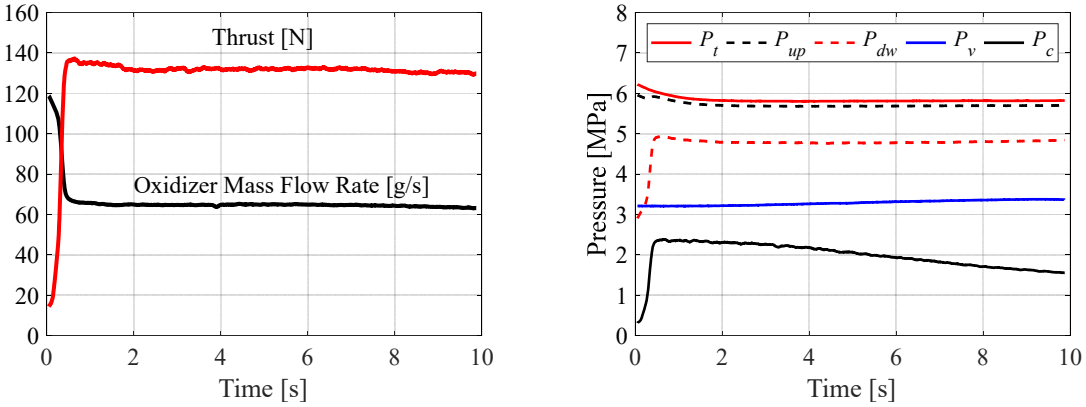

Fig. 4 Direct measurements of Test 2

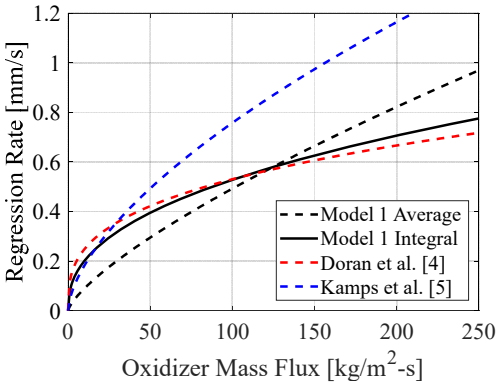

Fig. 5 Comparison of Model 1 with existing correlations

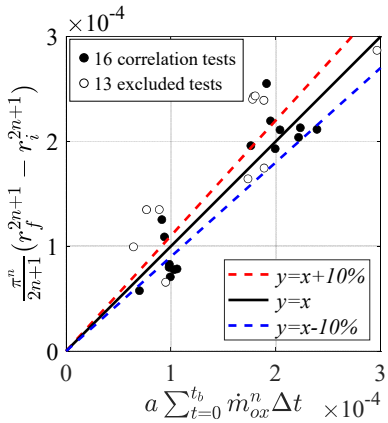

Fig. 6 Time-integral correlation of Model 1

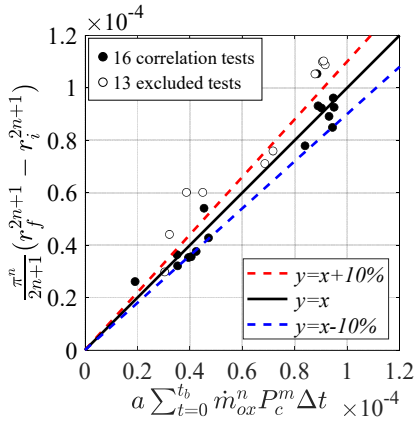

Fig. 7 Time-integral correlation of Model 2

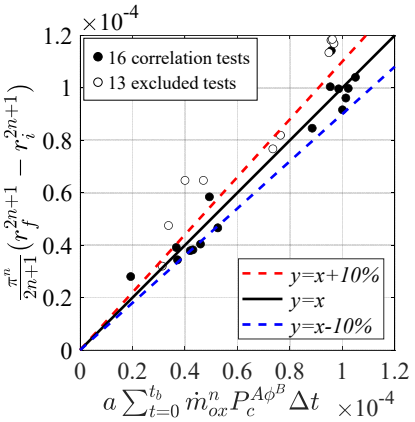

Fig. 8 Time-integral correlation of Model 3

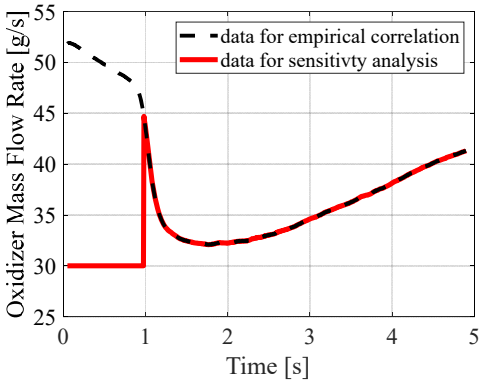

Fig. 9 The oxidizer mass flow rate history for sensitivity analysis (Test 16)